Structure of Amorphous Aluminum Oxide

Sung Keun Lee,[1,*] Sung Bo Lee,[2] Sun Young Park,[1] Yoo Soo Yi,[1] and Chi Won Ahn[3]
[1]*School of Earth and Environmental Sciences, Seoul National University, Seoul, 151-742 Korea*
[2]*School of Materials Science and Engineering, Seoul National University, Seoul, 151-742, Korea*
[3]*National Nanofab Center, KAIST, Daejeon 305-806, Korea*
(Received 9 April 2009; revised manuscript received 6 June 2009; published 24 August 2009)

Whereas prototypical Al_2O_3 is not a glass former, amorphous Al_2O_3 can be formed as thin films through vapor deposition and can serve as a structural model for the Al_2O_3 glass. The first two-dimensional solid-state NMR experiments for amorphous Al_2O_3 thin film reveal that four- and five-coordinated species are predominant (95%), while six-coordinated species are minor. Such a species distribution is remarkably similar to what has been predicted theoretically for Al_2O_3 melts. Upon annealing to 800 °C the five-coordinated species becomes negligible, indicating the onset of crystallization of Al_2O_3.

DOI: 10.1103/PhysRevLett.103.095501 PACS numbers: 61.43.Fs, 82.56.−b, 68.55.−a

Aluminum oxide (Al_2O_3) is one of the simplest covalent oxides and has received recent attention because Al_2O_3 thin films are used as supports for catalytic nanoparticles, gate microelectronic devices, and protective films with unique chemical durability and mechanical strength ([1,2] and references therein). The deposited Al_2O_3 thin film is often heat treated to form crystalline Al_2O_3 (Ref. [3]). The structure and surface stoichiometry of crystalline ultrathin alumina films are reported to be different from those of bulk Al_2O_3 (Refs. [1,4]) due to surface relaxation of the topmost Al_2O_3 layer [5] and various structural domains [2]. γ-Al_2O_3 has also been identified as the major phase in thin films [3]. While the studies cited here provided an improved understanding of the structure of crystalline thin films, as-deposited Al_2O_3 thin films obtained by physical vapor deposition are in the amorphous state as reported by earlier pioneering studies [3,6], and their structure has not yet been established.

Most of single-component covalent oxides such as SiO_2, GeO_2, and B_2O_3 are good glass formers, and the structure of prototypical oxide glasses remains a difficult problem in the physical sciences, leading to extensive experimental studies on the coordination number and the topology in the archetypal glasses formers (e.g., [7–10]). Prototypical Al_2O_3 alone, however, has not been classified as a glass former. The structure of pure Al_2O_3 glass, thus, has not been studied experimentally due to difficulties involved in its synthesis, particularly in quenching Al_2O_3 melts [11]. As amorphous phases can be formed as thin films through vapor deposition [3,12], study of amorphous Al_2O_3 thin films can be essential in understanding the as-yet-unknown structure of Al_2O_3 glass.

Conventional experimental probes used for studying the atomic configurations of crystals are not well suited for probing the structure of amorphous oxide thin film. Recent progress in solid-state NMR techniques including triple quantum magic angle spinning (3QMAS) NMR has yielded two-dimensional (2D) spectra [13], resolving structural details around quadrupolar nuclides (e.g., ^{27}Al, ^{17}O) in oxide glasses (e.g., [14]). Because the 2D NMR techniques require a relatively large amount of the sample and are suited for the study of bulk materials, obtaining a high signal-to-noise ratio for thin film surfaces is challenging and no 2D NMR technique has been applied to study the amorphous thin films. Here, we analyze the local atomic structures of amorphous Al_2O_3 thin films using 2D ^{27}Al 3QMAS NMR with optimized experimental conditions for thin film analysis and report the experimental evidence for coordination states in a vapor-deposited oxide thin film.

A 1.4-μm-thick Al_2O_3 thin film was deposited on a p-type boron-doped (B-doped) $Si_3N_4/Si(100)$ wafer by rf magnetron sputtering at 5×10^{-6} Torr using an Al_2O_3 target (99.995%) at an rf power of 500 W at room temperature in an Ar environment. After Al_2O_3 deposition, the opposite side of the substrate was etched using a KOH-water solution up to approximately 100 μm. Because the presence of surface Al-OH in the top surface layers is non-negligible only at a high P_{H_2O} condition ($>10^{-2}$ Torr) [15], the hydrogen content and its effect on the Al coordination environments in the film are likely to be negligible. Cross-section TEM studies showed no evidence of the presence of crystalline phases in the as-deposited alumina thin film (Fig. 1), indicating its amorphous nature. The chemical composition of the Ar ion etched thin film surfaces (approximately 30 nm below the surface) was analyzed using Al-2p and O-1s x-ray photoemission spectroscopy as the stoichiometry of crystalline Al_2O_3 ultrathin film deviates from its ideal composition at the top surface layers [1]. Taking into consideration the atomic sensitivity factor for Al and O from the α-Al_2O_3 reference (O/Al ratio of 1.698 ± 0.048 in our x-ray photoemission spectroscopy analysis), the O/Al atomic ratio of the Al_2O_3 thin film is 1.53 ± 0.054 ($= 1.734/1.698 \times 1.5$).

^{27}Al MAS and 3QMAS NMR spectra were collected on a Varian400 solid-state spectrometer (9.4 T) at a Larmor

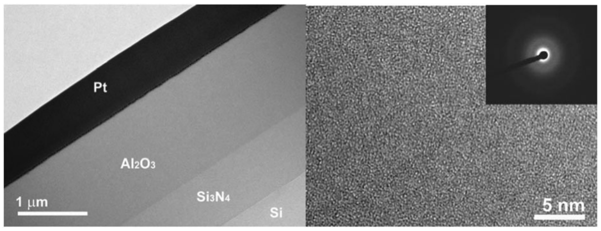

FIG. 1. Cross section TEM image [(left) low- and (right) high-resolution image with a diffraction pattern (inset)] of as-deposited alumina thin film. TEM specimens were prepared on a focused Ga-ion beam (FIB) workstation. Cross section image of lamellae, $\sim$10 μm wide and 5 μm deep, lifted out and attached to a Mo half grid. The cutting of the lamellae was done with 7–20 nA at 30 kV. The specimens were milled at 30 kV and 0.5–3 nA and were polished at 5 kV and 70 pA to reduce focused-Ga-ion-beam-induced damage. The final thickness was 40–50 nm. The image was obtained in a TEM [JEM4010 (JEOL Ltd., Co.)].

frequency of 104.23 MHz using a 3.2 mm zirconia rotor in a Varian double-resonance probe. The recycle delay for the NMR experiments was 1 s, with the rf pulse length being 0.3 μs (flip angle of $\sim 15°$ for the central transition in solids) for the 1D MAS. Ninety-six thousand to 230 400 scans were averaged in the ^{27}Al MAS NMR spectra.

To remove residual anisotropic spectral broadening in 1D MAS due to the 2nd order quadrupolar interaction (2QI) between quadrupolar moment and electric field gradient, the 3QMAS technique utilizes the correlation between the 3Q ($3/2 \leftrightarrow -3/2$) and single quantum (1Q) coherences ($1/2 \leftrightarrow -1/2$): the frequencies for both coherences ($\omega_{1/2\leftrightarrow-1/2}$, $\omega_{3/2\leftrightarrow-3/2}$) have similar 2QI dependence with known scaling coefficients ($C_{1/2\leftrightarrow-1/2}$, $C_{3/2\leftrightarrow-3/2}$). The pulse sequence can be designed to achieve a selection of 3Q for a t_1 period and subsequent 1Q coherences for $kt_1(k = C_{3/2\leftrightarrow-3/2}/C_{1/2\leftrightarrow-1/2})$ [13]. This removes the 2QI, enhancing resolution among atomic sites. At the end of kt_1, coherence decay is recorded during t_2. The resulting 2D NMR (t_1, t_2) data collected by incrementing t_1 were Fourier transformed to produce spectra that are isotropic in the w_1 dimension (free of 2QI) and that portray distorted MAS spectra in the w_2 dimension (the MAS dimension) [14,16]. The ^{27}Al 3QMAS NMR spectrum was collected using a fast-amplitude modulation based shifted-echo pulse sequence (consisting of two hard pulses with durations of 3.0 and 0.6 μs and a soft pulse with a duration of 15 μs), which enhances signal intensity compared with the result without fast-amplitude modulation implementation. The spinning speed should be larger than 17 kHz at 9.4 T, making a standard 3.2 mm rotor suitable for the thin film analysis. To achieve current signal-to-noise ratio in the 2D spectra, about 16 days of collection time were required. The spectra were referenced to a 0.1 M $AlCl_3$ solution.

Figure 2 presents the ^{27}Al MAS NMR spectra of the Al_2O_3 thin film (with the substrate) where the features at approximately 60, 35, and 0 ppm were observed. These features are likely due to distinct Al coordination environments such as four-, five-, and six-coordinated aluminums (i.e., $^{[4]}$Al, $^{[5]}$Al, and $^{[6]}$Al). The number of Al nuclides in a Al_2O_3 film (1.4-μm) on a 100-μm-thick Si p-type substrate with Al dopants is very small, and thus the effect of Al impurities in the substrate and/or the zirconia NMR rotor should be examined. The ^{27}Al MAS NMR spectrum of the empty rotor shows signals due to the Al background ($^{[6]}$Al). An insignificant but detectable amount of aluminum impurity in both $^{[4]}$Al ($\sim$60 ppm) and $^{[6]}$Al ($\sim$0 ppm) phases is observed in the Si substrate (Fig. 2, top). The spectrum obtained after subtraction of these background signals shows distinct Al features for $^{[5]}$Al, thereby confirming that these signals are due to the thin film (Fig. 2, bottom). The shapes of the peaks are not consistent with those of any of the crystalline Al_2O_3 polymorphs with known ^{27}Al NMR patterns where only peaks due to $^{[4]}$Al and $^{[6]}$Al are expected [17,18], indicating its amorphous nature as shown in Fig. 1. Because the features in the 1D ^{27}Al MAS NMR largely overlap and could also stem from the quadrupolar patterns corresponding to Al sites, 2D ^{27}Al 3QMAS NMR spectra without quadrupolar broadening are necessary.

Figure 3 shows the ^{27}Al 3QMAS NMR spectrum for the Al_2O_3 thin film. Three Al coordination environments (mostly $^{[4,5]}$Al and a small fraction of $^{[6]}$Al) are clearly resolved. These results confirm that the changes in the peak

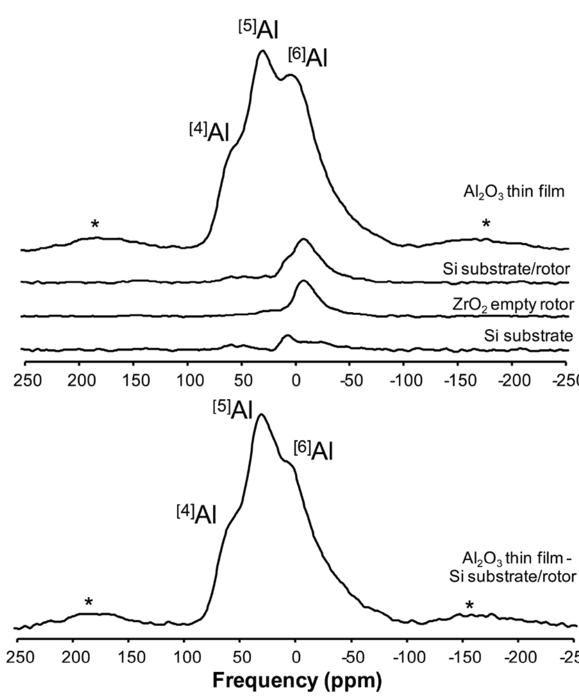

FIG. 2. ^{27}Al MAS NMR spectra for Al_2O_3 thin film, rotor background, and Si substrate. * refers to spinning sidebands.

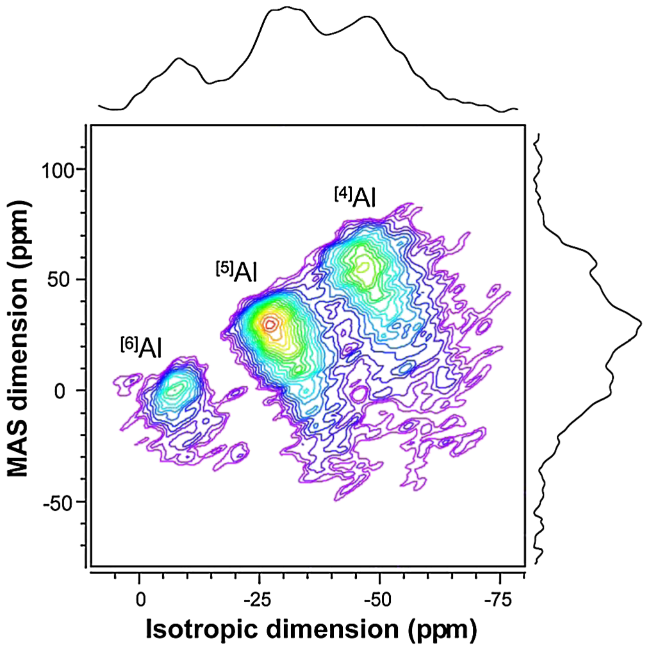

FIG. 3 (color online). ^{27}Al 3QMAS NMR spectra for Al_2O_3 thin film. Projections on the isotropic and MAS dimension are also shown. Contour lines are drawn at 5% intervals from relative intensities of 12% to 97% with added lines at 6% and 9%.

shape of the ^{27}Al MAS NMR spectrum (Fig. 2) stem from changes in the Al coordination states. The presence of a significant amount of $^{[5]}$Al confirms the amorphous nature of the Al_2O_3 thin film. Because the 3QMAS NMR signal intensity is not quantitative and depends on the magnitude of quadrupolar interactions of Al sites [14], the $^{[n]}$Al fractions are calibrated by taking into account the uneven multiple quantum transition process for each $^{[n]}$Al due to the magnitude of the quadrupolar interactions, experimental conditions, and the percentage of Al impurity in the substrate. The calibrated fractions for $^{[4]}$Al, $^{[5]}$Al, and $^{[6]}$Al are 55% ± 3%, 42% ± 3%, and 3% ± 2%, respectively; the estimated $^{[6]}$Al fraction was about 11%, but a major portion of the Al peak stems from the rotor backgrounds plus Al dopants in the substrate (Fig. 2). Thus, by subtracting the estimated peak volume for $^{[6]}$Al in the impurity and dopants (about 8%–9%), the resulting $^{[6]}$Al fraction can be estimated at 2%–3%. These fractions show a remarkable similarity to those reported for Al_2O_3 melts in molecular dynamics simulations [19,20]. The average coordination number of Al_2O_3 melts suggested by high-temperature NMR studies is ~4.5 (Ref. [21]), similar to that obtained in the present NMR analysis. Whereas future synchrotron x-ray scattering studies may provide information about the average coordination number of amorphous Al_2O_3 thin film, the x-ray scattering study of alumina melts shows that the $^{[4]}$Al-O, $^{[5]}$Al-O, and $^{[6]}$Al-O correlation peaks in radial distribution function overlap [19]. The $^{[4,5,6]}$Al peaks in the thin film are, however, well resolved in the Al-27 3QMAS NMR spectra (Fig. 3), yielding unambiguous coordination environments.

The center of gravity of the peak in the ^{27}Al 3QMAS NMR spectrum for the thin film was used to obtain a structurally relevant quadrupolar coupling product (P_q). The P_q value, a measure of lattice distortion, decreases with an increase in the Al coordination number from 7.1 ± 0.3 MHz for $^{[4]}$Al, 6.2 ± 0.3 MHz for $^{[5]}$Al, and 4.5 ± 0.3 MHz for $^{[6]}$Al. These P_q values are larger for amorphous thin films than for aluminosilicate glasses at 1 atm and high pressure [16], indicating significant distortion of the Al sites. We note that there could exist other Al sites (possibly of $^{[6]}$Al) with large P_q values (>7–8 MHz, see below) in the film as the intensity of these sites can be underestimated in the 3QMAS NMR. As the atomic structures of Al_2O_3 melts and glasses have not been experimentally confirmed, the current 2D ^{27}Al NMR spectra obtained for amorphous thin films provide information on the structure of Al_2O_3 glass and melts.

To gain insights into the temperature-induced structural changes in the Al_2O_3 thin film, we annealed the film at 800 °C and 1200 °C for 2 h. The ^{27}Al MAS NMR spectrum of the annealed Al_2O_3 thin film differs from that of the as-deposited thin film (Fig. 4, after background subtraction). The $^{[5]}$Al content became negligible upon annealing at 800 °C; hence, at this stage, the NMR spectrum showed only $^{[4]}$Al and $^{[6]}$Al peaks, indicating the onset of crystallization of Al_2O_3. The peak patterns in the ^{27}Al MAS NMR spectra were similar to those of crystalline transitional γ- and/or θ-Al_2O_3 (e.g., [17,18]), and the crystallization scheme is consistent with that predicted by recent studies on bulk Al_2O_3 (Ref. [22]). In the spectrum of the thin film annealed at 800 °C, the peak widths for $^{[4]}$Al were large owing to the relatively large P_q (~6 MHz) of crystalline

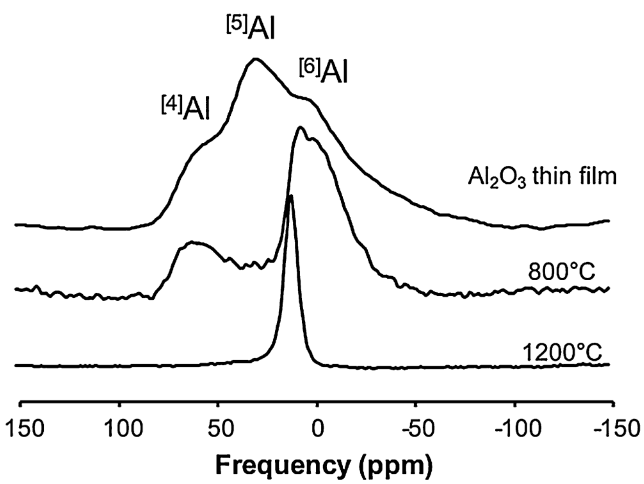

FIG. 4. ^{27}Al MAS NMR spectra for Al_2O_3 thin film annealed at 800 °C and 1200 °C. Rotor/Si backgrounds were subtracted from the original spectra.

γ-Al_2O_3 (Ref. [18]). The NMR spectrum obtained after annealing at 1200 °C showed a sharp peak due to $^{[6]}$Al at approximately 12–13 ppm, which corresponded to the α-Al_2O_3 phase. The decrease in peak width with temperature indicates an increase in the local symmetry and topological order, as is the case of other types of bulk Al_2O_3, Al nanoparticles, and anodically oxidized porous Al films [23–25]. The mechanism related to the annihilation of $^{[5]}$Al during the transformation of amorphous Al_2O_3 to crystalline Al_2O_3 can be described by the following scheme: $2^{[5]}\mathrm{Al} \Rightarrow {}^{[4]}\mathrm{Al} + {}^{[6]}\mathrm{Al}$. This mechanism involves the formation of edge-sharing Al octahedrons from corner-sharing $^{[5]}$Al. While the Al-27 MAS NMR (Fig. 2) shows that the NMR signal from the thin film is weak and thus comparable to the contribution from the Al dopants in the substrate, necessitating background subtraction, 1D MAS NMR is more efficient than the 2D 3QMAS NMR technique. Thus if the origins of the features in Al-27 MAS NMR are known, 1D MAS NMR allows us to investigate the effect of temperature on the structure (Fig. 4).

Because the crystal structure of the ultrathin alumina thin film (with several Å thickness) is different from those of bulk alumina polymorphs, the top few surface layers in the amorphous alumina thin film would be different from those of the 1.4 μm amorphous thin film studied here. While the current sensitivity of solid-state NMR does not allow us to probe Al nuclides in the top few surface layers of ultrathin alumina thin film yet, it should be noted that the results of ongoing NMR study on the atomic layer deposited thin film (with thickness of ~0.2 μm) provide further insights into the effect of thickness and deposition methods on the coordination environments.

The high $^{[5]}$Al content in amorphous Al_2O_3 is indicative of a large number of oxygen triclusters (oxygen coordinated by three aluminums, $^{[3]}$O), as suggested by the molecular dynamics simulations of Al_2O_3 melts [19,20]. It has been experimentally shown that $^{[3]}$O occurs in other archetypal oxide glasses at high pressures [26]. A significant fraction of $^{[3]}$O in the thin film at 1 atm implies a modification of a traditional view of glass structure based on a random network model that only allows $^{[2]}$O. Such framework cation and oxygen species distributions in the melts are known to be largely responsible for their macroscopic properties (e.g., [26,27]). Considering the similarity between the structure of the Al_2O_3 melt and that of the amorphous phase, our spectroscopic results yield improved understanding of the atomistic origins of the microscopic dynamics of Al_2O_3 melts [28].

In conclusion, we reported the direct experimental evidence for the coordination states of vapor-deposited amorphous Al_2O_3 thin film using 2D solid-state NMR. In amorphous Al_2O_3 the fractions for $^{[4]}$Al, $^{[5]}$Al, and $^{[6]}$Al are 55% $\pm$ 3%, 42% $\pm$ 3%, and 3% $\pm$ 2%, respectively. Such a species distribution is similar to what has been predicted theoretically for Al_2O_3 melts [19,20]. The current study highlights the first application of ^{27}Al 2D NMR to obtain a detailed structure of thin film. The effects of temperature, type of substrate, and other processing conditions on the structure of Al_2O_3 glass remain to be explored. The results shed light on a new opportunity to analyze the structure of diverse crystalline and amorphous thin film oxides and to clarify unknown details of the structures of a new class of vapor-deposited oxide glasses that would otherwise be difficult to synthesize.

S. K. L. acknowledges the support of the National Research Foundation (NRF) of Korea (2007-000-20120), which provided the main support of this work. S. B. L. acknowledges support for thin film preparation by the NRF (2008-314-D00176). We thank two reviewers for constructive suggestions.

*sungklee@snu.ac.kr

[1] G. Kresse *et al.*, Science **308**, 1440 (2005).
[2] A. Stierle *et al.*, Science **303**, 1652 (2004).
[3] T. C. Chou *et al.*, Thin Solid Films **205**, 131 (1991).
[4] C. Freysoldt, P. Rinke, and M. Scheffler, Phys. Rev. Lett. **99**, 086101 (2007).
[5] C. Barth and M. Reichling, Nature (London) **414**, 54 (2001).
[6] R. Dupree *et al.*, J. Phys. (Paris) **46**, 113 (1985).
[7] M. Guthrie *et al.*, Phys. Rev. Lett. **93**, 115502 (2004).
[8] S. K. Lee *et al.*, Nature Mater. **4**, 851 (2005).
[9] R. E. Youngman *et al.*, Science **269**, 1416 (1995).
[10] T. Sato and N. Funamori, Phys. Rev. Lett. **101**, 255502 (2008).
[11] A. Rosenflanz *et al.*, Nature (London) **430**, 761 (2004).
[12] S. F. Swallen *et al.*, Science **315**, 353 (2007).
[13] I. Frydman and J. S. Harwood, J. Am. Chem. Soc. **117**, 5367 (1995).
[14] J. H. Baltisberger *et al.*, J. Am. Chem. Soc. **118**, 7209 (1996).
[15] J. A. Kelber, Surf. Sci. Rep. **62**, 271 (2007).
[16] S. K. Lee, J. Phys. Chem. B **108**, 5889 (2004).
[17] B. A. Huggins and P. D. Ellis, J. Am. Chem. Soc. **114**, 2098 (1992).
[18] D. Coster, A. L. Blumenfeld, and J. J. Fripiat, J. Phys. Chem. **98**, 6201 (1994).
[19] S. Ansell *et al.*, Phys. Rev. Lett. **78**, 464 (1997).
[20] S. Jahn and P. A. Madden, J. Non-Cryst. Solids **353**, 3500 (2007).
[21] B. T. Poe *et al.*, J. Phys. Chem. **96**, 8220 (1992).
[22] T. C. Chou and T. G. Nieh, Thin Solid Films **221**, 89 (1992).
[23] I. Farnan *et al.*, Thin Solid Films **173**, 209 (1989).
[24] H. J. Kim, H. C. Lee, and J. S. Lee, J. Phys. Chem. C **111**, 1579 (2007).
[25] J. A. Wang *et al.*, J. Phys. Chem. B **103**, 299 (1999).
[26] S. K. Lee *et al.*, Proc. Natl. Acad. Sci. U.S.A. **105**, 7925 (2008).
[27] J. L. Yarger *et al.*, Science **270**, 1964 (1995).
[28] H. Sinn *et al.*, Science **299**, 2047 (2003).